Bulletin of the Seismological Society of America, Vol. 92, No. 4, pp. 1423–1432, May 2002

Early Postseismic Deformation from the 16 October 1999 M_w 7.1 Hector Mine, California, Earthquake as Measured by Survey-Mode GPS

by S. Owen, G. Anderson, D. C. Agnew, H. Johnson, K. Hurst, R. Reilinger, Z.-K. Shen, J. Svarc, and T. Baker

Abstract The 16 October 1999 (M_w 7.1) Hector Mine earthquake was the largest earthquake in California since the 1992 (M_w 7.3) Landers event. The Hector Mine earthquake occurred in the eastern Mojave Desert, where the density of permanent Global Positioning System (GPS) stations is relatively low. Since the earthquake, groups from the United States Geological Survey, University of Southern California, University of California, Los Angeles, University of California, San Diego, and Massachusetts Institute of Technology have made postseismic survey-mode observations to increase the spatial coverage of deformation measurements. A total of 55 sites were surveyed, with markers from a few meters to 100 km from the surface rupture. We present velocity estimates for the 32 sites that had enough repeated observations between 17 October 1999 and 26 March 2000 to provide reliable results; these survey-mode data complement the temporal and spatial coverage provided by newly installed Southern California Integrated Geodetic Network permanent GPS stations and future Interferometric Synthetic Aperture Radar postseismic results. We then use the postseismic velocity estimates to compute a simple afterslip model. Results of inversions show that the observed velocities are consistent with deep afterslip occuring underneath the coseismic rupture area.

Introduction

The 16 October 1999 (M_w 7.1) Hector Mine earthquake ruptured only 20 km to the east of the 1992 (M_w 7.3) Landers earthquake in a region of the Mojave Desert that experiences large earthquakes approximately every 10,000 years (Rockwell *et al.*, 2000; Lindvall *et al.*, 2001; Rymer *et al.*, 2002). In response to this earthquake, a team of researchers from five institutions collected data at 39 geodetic markers in the first 2 weeks following the earthquake. The coseismic Global Positioning System (GPS) displacements generated from these and other initial postseismic measurements are discussed in Hurst *et al.* (2000) and Agnew *et al.* (2002).

While it is well known that major earthquakes cause aseismic deformation transients, the mechanisms behind these transients are the subject of some debate (Savage and Svarc, 1997; Deng *et al.*, 1998; Pollitz *et al.*, 2000; Reilinger *et al.*, 2000). For this reason, there was a concentrated effort to collect both survey-mode and continuous GPS measurements of the postseismic deformation following the Hector Mine rupture. By analyzing the spatial and temporal distribution of the deformation, we potentially can resolve whether deformation in the lower crust is distributed or confined to narrow shear zones that extend below faults in the brittle crust. Two-dimensional calculations show that these competing models produce similar surface deformation (Savage, 1990), but by acquiring precise measurements with enough spatial and temporal coverage to go beyond simple two-dimensional models, we can begin to distinguish between different theories of how deformation is distributed (Pollitz *et al.*, 2000). The Hector Mine earthquake presents an ideal opportunity for applying recent advances in geodetic techniques to this problem.

Data

Teams from the United States Geological Survey (USGS), University of Southern California (USC), University of California, Los Angeles (UCLA), University of California, San Diego (UCSD), and Massachusetts Institute of Technology (MIT) made repeated survey-mode observations at a total of 55 sites following the earthquake, including sites on and off the Marine Corps Air Ground Combat Center (MCAGCC) (Fig. 1). In addition to observations at preexisting marks, we increased the density of the network around the Hector Mine earthquake by adding observations at new

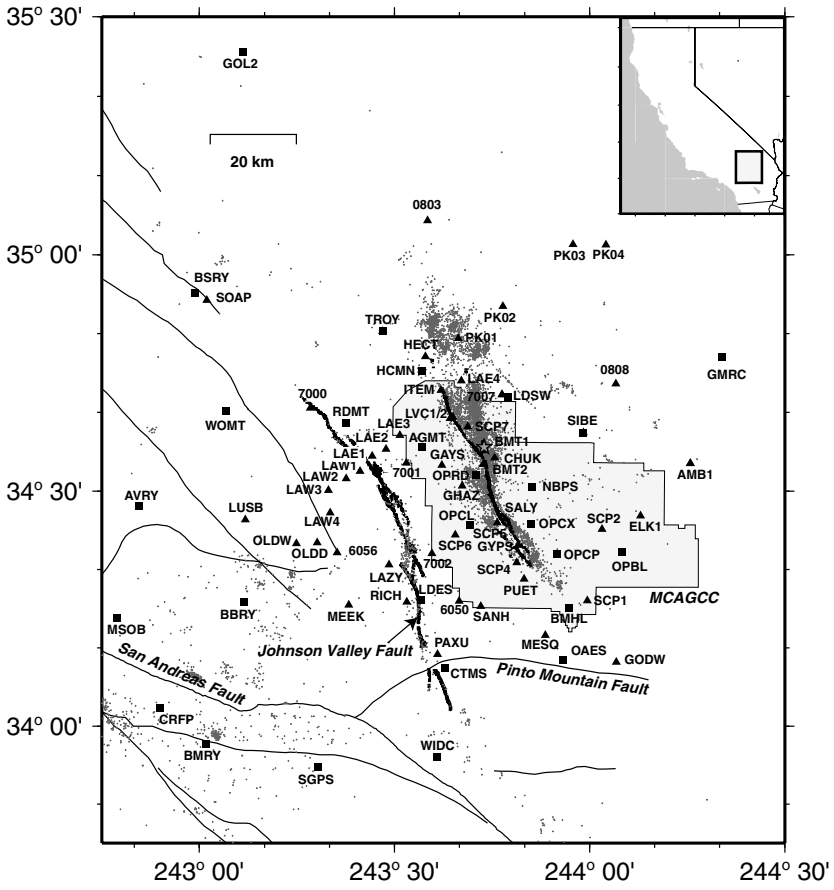

Figure 1. Map of survey-mode (triangles) and continuous (squares) GPS stations around the 1999 Hector Mine rupture. The Hector Mine and Landers surface ruptures are plotted in bold lines. Also shown are the locations of aftershocks, from 16 October 1999 through 26 March 2000, and the main-shock epicenter (star).

bench marks close to the surface rupture (stations LVC1, LVC2, BMT1, and BMT2 installed by UCLA) and installed new bench marks to extend a USGS profile placed perpendicular to the fault at the northern edge of the surface rupture (stations PK01–PK04 installed by UCSD; Fig. 1). Station density is greater on the west side of the Hector Mine rupture because of the work done following the Landers earthquake.

All groups used Ashtech Z-12 receivers and choke-ring antennas, the same receivers and antennas as used on the Southern California Integrated Geodetic Network (SCIGN) continuous installations. Several days of data were collected per occupation at most of the sites but at least 6 hours in all cases. The sites were revisited with varying frequency, ranging from the semicontinuous operations at stations TROY and SIBE to only two postseismic observations at several sites by the end of March 2000. For sites with only a few very short occupations, the uncertainties in their velocity estimates were so large that they could not determine a useful postseismic velocity, so there are fewer velocities shown than there are stations in Figure 1. Over the next few years, all of these sites will have enough observations to calculate meaningful velocity estimates.

There were a few continuous GPS sites (e.g., OAES and LDES) operating close enough to the Hector Mine rupture to capture the very early postseismic transient. Beginning immediately after the earthquake, the SCIGN group installed more continuous GPS sites around the Hector Mine rupture, as discussed in detail in Hudnut *et al.* (2002).

We processed both the survey-mode data and data from these SCIGN sites using the GIPSY–OASIS II point-positioning software (Zumberge *et al.*, 1997), using the point_amb software written by K. Hurst to fix ambiguities. We computed all solutions using nonfiducial orbits and clocks generated by the Jet Propulsion Laboratory; we transformed all positions and covariances into the International Terrestrial Reference Frame 1997 (Boucher *et al.*, 1999). The positions and model estimates plotted in Figure 2 and the velocities plotted in subsequent figures are shown relative to the SCIGN station BLYT, a site 150 km to the east of the surface rupture.

We computed the average velocity estimates for two time periods: 17 October–30 November 1999 and 17 November–26 March 2000; we chose the time periods based on the decay of the early rapid postseismic transient seen in the continuous time series (Hudnut *et al.*, 2002) and on the availability of survey-mode measurements. Survey-mode sites visited in the last 2 weeks of November are included in both estimates. We estimated the velocities using a weighted least-squares inversion. Both time periods are fit well by a constant-velocity model, without any additional

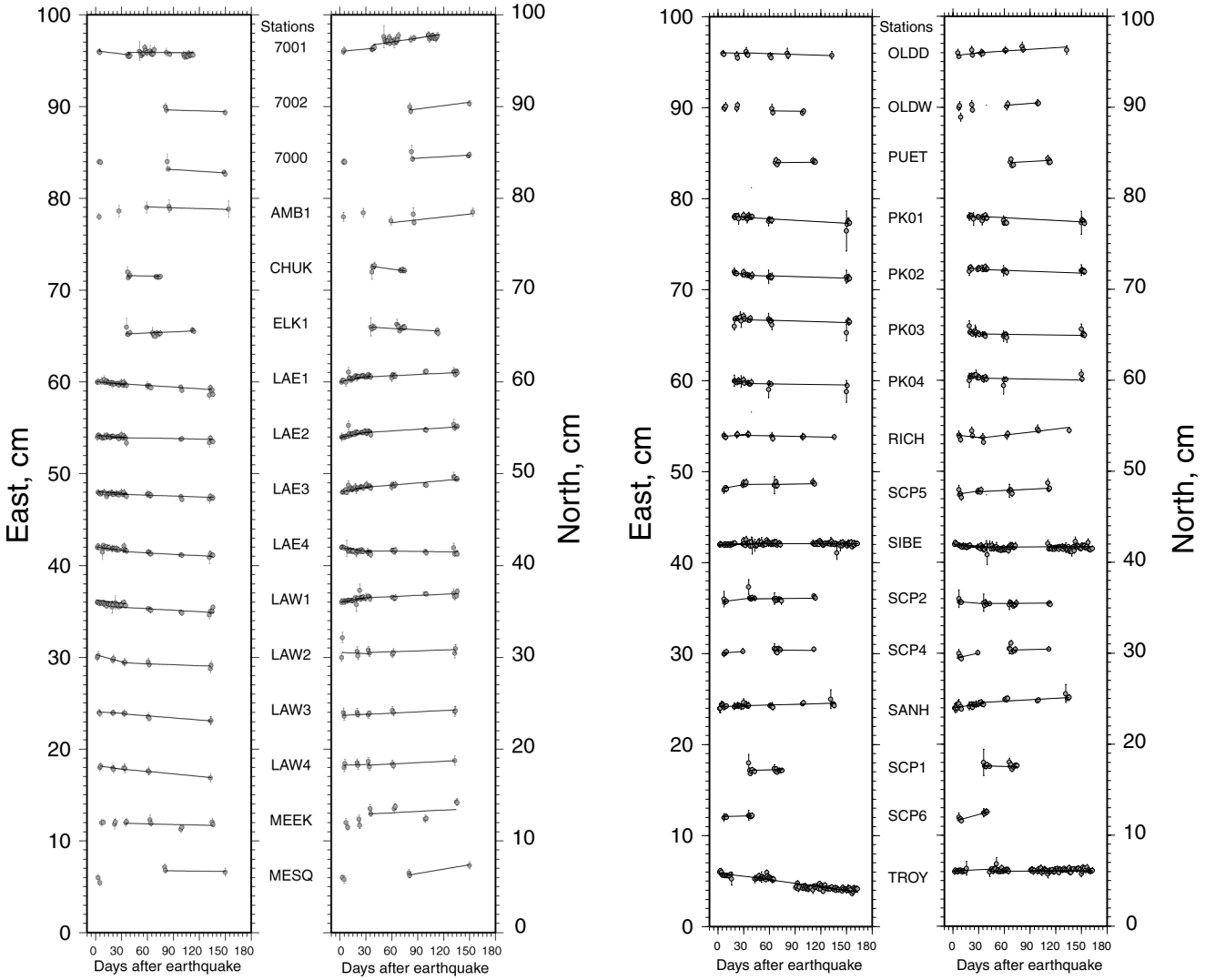

Figure 2. Time series of survey-mode data collected since the Hector Mine earthquake. Error bars represent two-sigma error values. Lines represent the two velocity models. Some stations were not included in both velocity models and so do not have a model for the entire time period. Stations plotted in numerical/alphabetical order.

scaling of the GPS formal errors; the chi-square values of the October–November and the November–March velocity estimates are 0.94 and 1.4, respectively. We scaled our error estimates by this misfit to a constant-velocity model, so that the chi-square value is 1.0 for both velocity estimates. There are large differences in the error ellipses between stations; the survey-mode sites have larger errors than the continuous sites because the former have fewer observations, their observation durations occasionally are less than 24 hours, and they usually span a slightly shorter time period. The velocity estimates for survey-mode sites will become more accurate over time.

In Figures 3 and 4, stations close to the San Andreas fault show velocities that are the result of secular strain, not postseismic transients. Before using these velocities to model postseismic slip distributions, we accounted for the secular strain by subtracting the estimated secular velocities at these sites, which we estimated by assuming a 30 mm/yr slip rate along the San Andreas fault and a locking depth of 15 km. The resulting postseismic velocities used to calculate afterslip models (Fig. 5) are shown in Figures 6a and 7a. Only sites close to the San Andreas fault were affected by this correction.

Deep-Afterslip Model

We used our postseismic velocity estimates to test the hypothesis that there is a significant amount of afterslip along the coseismic rupture plane or extensions of this fault. We estimated how much of the postseismic deformation signal can be explained by afterslip by calculating the slip distribution across a series of square dislocations (4 km $\times$

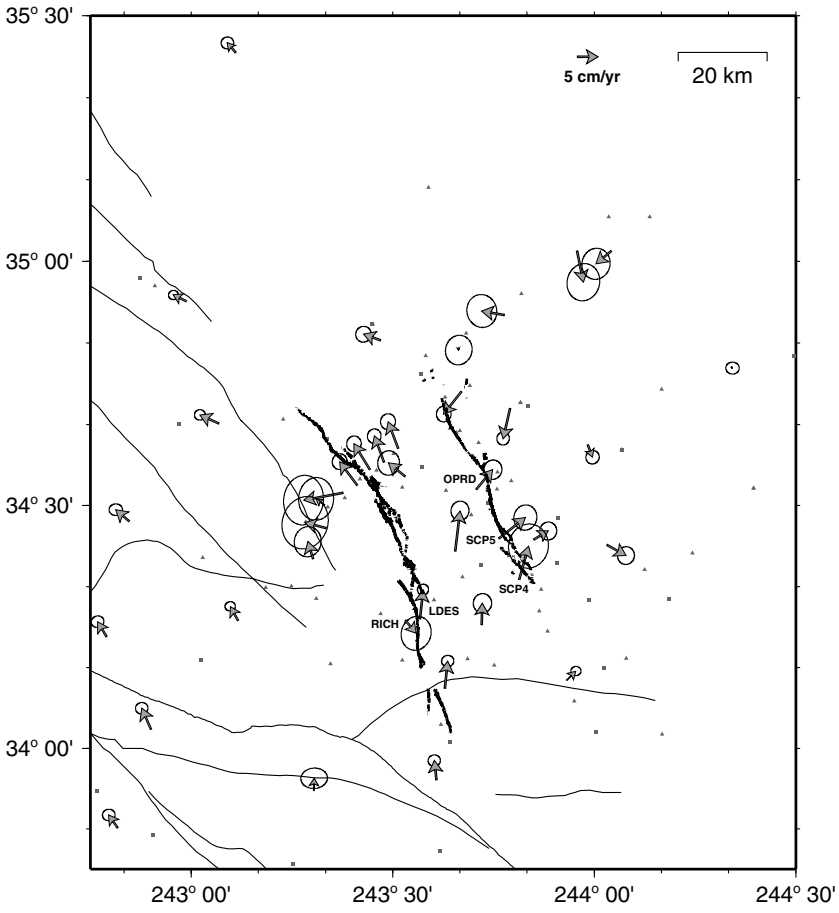

Figure 3. Average postseismic velocities from 17 October through 30 November 1999. Error ellipses represent 95% confidence values. Triangles and squares mark the location of all sites within the figure for which there are postseismic measurements by the end of March. A complete map of station names is given in Figure 1.

4 km) in a homogeneous elastic half-space (Okada, 1985). We used a geometry based on the mapped surface rupture of Treiman *et al.* (2002); we extended the fault to 40 km depth and by ~20 km on each end, following a trend roughly consistent with the aftershocks (Hauksson *et al.*, 2002) (see Fig. 1). A finite-difference approximation of the Laplacian equation is used to apply smoothing constraints. These smoothing constraints prevent the inversion from generating solutions with unreasonably varied slip values from fault patch to fault patch.

Since this is an underdetermined problem and many different models will fit the data, we need to evaluate the model based on both data fit and reasonableness of the model. We employed a singular-value decomposition (e.g., Harris and Segall, 1987) to generate a starting model and then used a bounded-variable least-squares inversion (Stark and Parker, 1995) to estimate the final model. This method constrains the slip values to be right-lateral and avoids the left-lateral values commonly calculated with only a singular-value decomposition inversion. In the models shown here, we constrained the slip distribution to approach zero values at all four edges of the fault. The estimated slip distributions for the two time periods are shown in Figure 5. The model-predicted velocities and residual velocities, or unmodeled signal, are shown in Figures 6 and 7.

Discussion

While not as dramatic as the time series from continuous stations, some of the survey-mode stations do show a change in the displacement rate over the October–March time period. The USGS profile sites east of the Landers rupture (LAE1–LAE4) were observed continuously for the first 30 days after the earthquake, and the slope over the first 30 days is visibly steeper than the slope from the remaining observations (Fig. 2a). The decay in the velocities over the first 160 days after the earthquake also is apparent by comparing Figures 3 and 4. The maximum velocities in Figure 3 are on the order of ~10 cm/yr, while the maximum velocities in Figure 4 are ~5 cm/yr (these velocities are plotted at different scales to best represent the velocity field in each time period). This decrease in velocities is comparable to what was observed following the Landers earthquake (Shen *et al.*, 1994).

The initial postseismic velocities (Fig. 3) show continued right-lateral motion about the surface rupture. The density of the station coverage is fairly poor for testing if the deformation is symmetric about the surface rupture, but the velocities are roughly the same, taking into consideration that secular motion causes an increase in north-northwest velocities from east to west. There is some significant fault-

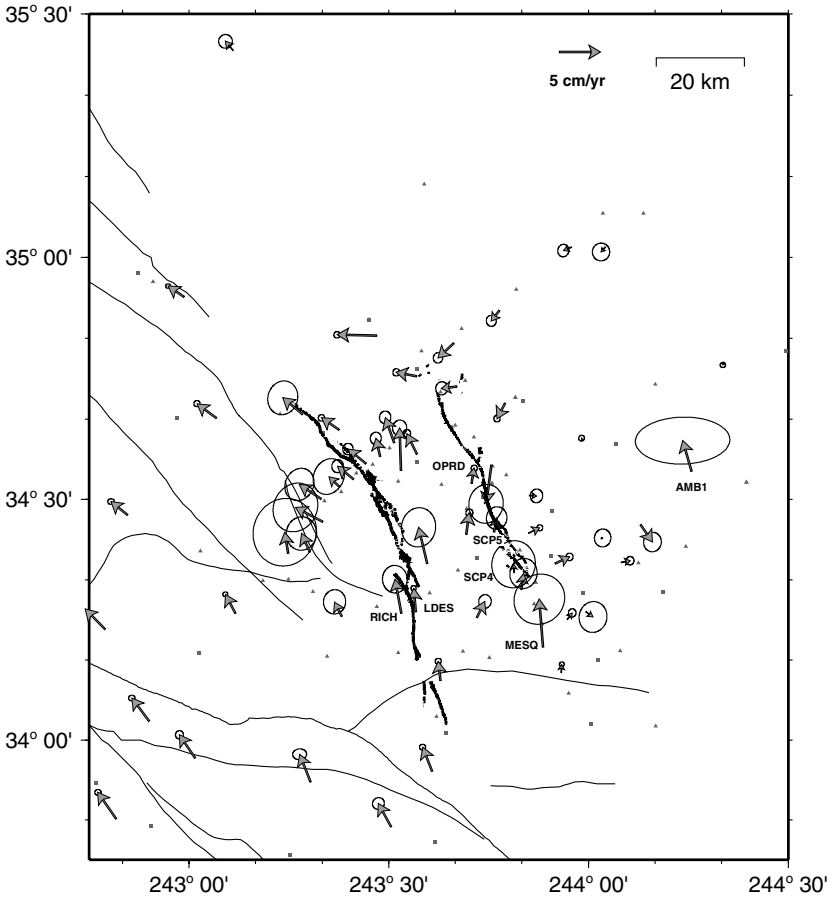

Figure 4. Average postseismic velocities from 17 November 1999 through 26 March 2000. Error ellipses represent 95% confidence values. Triangles and squares mark the location of all sites within the figure for which there are postseismic measurements by the end of March. A complete map of station names is given in Figure 1.

perpendicular motion at three stations on the west side of the rupture (OPRD, SCP5, and SCP4), which motion may be consistent with some localized fault movement or perhaps poroelastic rebound; fault-perpendicular shortening was observed and interpreted as poroelastic rebound following the Landers earthquake (Peltzer *et al.*, 1998). The maximum velocities that are consistent with a right-lateral slip pattern are observed ~10–20 km away from the fault. If we assume that this deformation is caused by fault slip on the coseismic rupture plane or its extensions, the location of the maximum velocities indicates that the source of the deformation has to be at some depth and cannot be entirely caused by shallow afterslip.

The average velocities from a month after the earthquake through March 2000, though slower than those for the first month, have smaller error ellipses on average. During this later period, we have an increased density of stations due, in part, to more survey-mode sites having reasonable velocities and, in part, to the new continuous-monitoring sites installed by SCIGN after November 1999 (Hudnut *et al.*, 2002). The velocities are still consistent with predominantly right-lateral motion. Over this later period, the fault-perpendicular component is much smaller at stations OPRD, SCP5, and SCP4. Apart from a few survey-mode stations that have anomalous velocities compared with nearby sites (MESQ and AMB1), the maximum velocities are still 10–20 km away from the surface rupture.

While GPS stations are, in general, too sparsely distributed to detect small-scale fault motion off the main rupture, the stations LDES (a continuous site) and RICH (a survey-mode site) have significantly different velocities in both velocity estimates, and they are separated by the Johnson Valley fault segment of the Landers rupture. Interferometric Synthetic Aperture Radar (InSAR) phase gradients show evidence of small-scale triggered slip on faults surrounding the Landers rupture (Price and Sandwell, 1998). Postseismic interferograms and phase-gradient maps can be used to confirm whether the difference in velocities between LDES and RICH is due to fault slip or monument or measurement problems with the survey-mode site RICH.

The afterslip models shown in Figure 5 indicate that postseismic deformation is consistent with deep afterslip occurring underneath the coseismic rupture area. This result is consistent with the results from recent major strike-slip earthquakes, such as the *M* 7.3 Landers earthquake (Savage and Svarc, 1997) and the *M* 7.5 Izmit, Turkey, earthquake (Reilinger *et al.*, 2000), where the strongest postseismic afterslip was seen beneath the main ruptures. By splitting the data into two different time periods, we can begin to test for temporal changes in the afterslip distribution. There is a de-

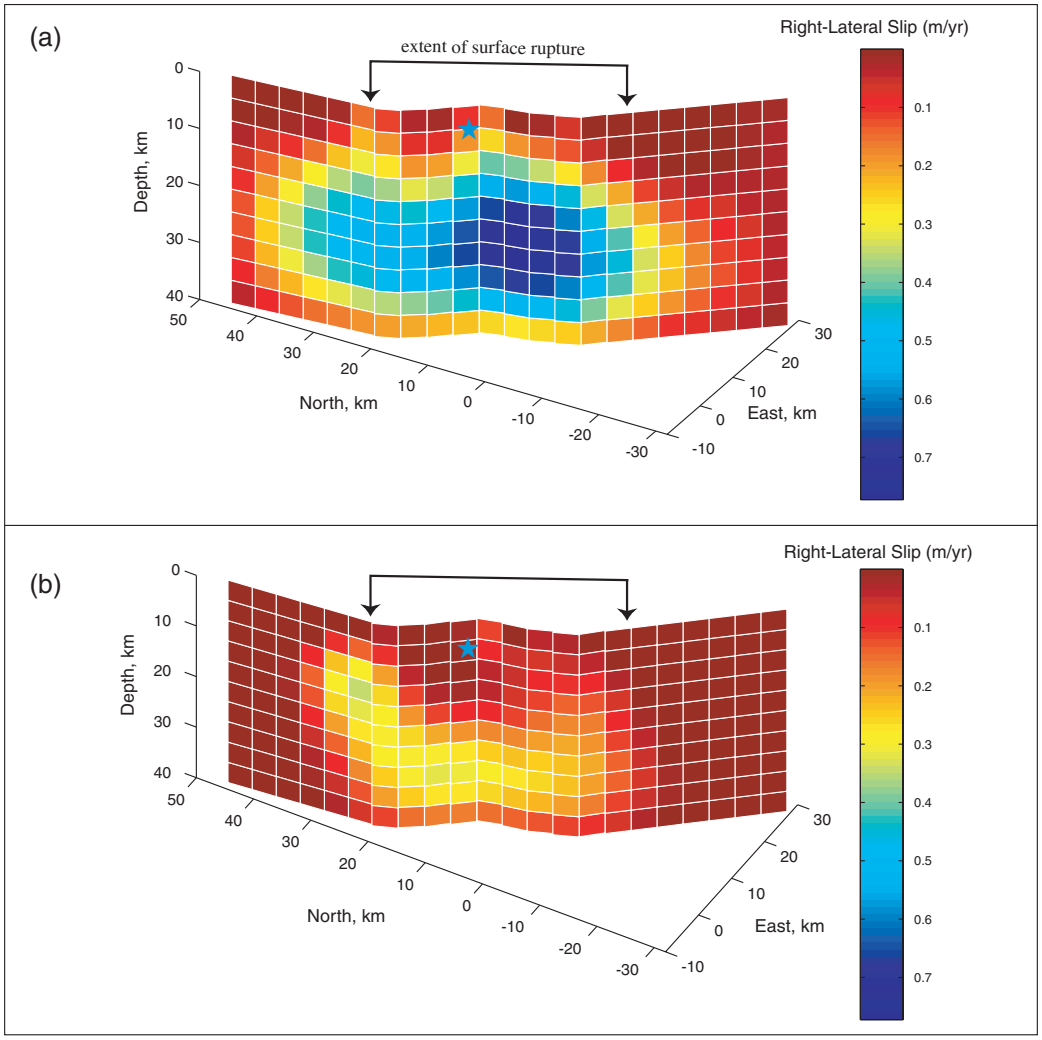

Figure 5. Deep-afterslip model results: (a) Slip distribution based on the October–November 1999 velocity estimate and (b) slip distribution based on the November 1999–March 2000 velocity estimate. The epicenter of the earthquake is indicated by the blue star.

crease in slip rate between Figure 5a and 5b, with only the fault-plane area north of the coseismic rupture continuing to slip at rates comparable to the October–November rates. The area with the maximum slip rate also shifts northward in the November–March model. Analysis of data after March 2000 and including results from InSAR will help to resolve this apparent northward shift more precisely.

Summary

Survey-mode GPS data collected after the Hector Mine earthquake show postseismic velocities consistent with continued right-lateral motion. The maximum rates of postseismic motion from both continuous and survey-mode GPS decay from ~10 cm/yr over the first 30 days to ~5 cm/yr over the following 130 days. Surface velocities show continued right-lateral motion, with the highest velocities observed ~10–20 km from the surface rupture. The estimated slip distributions from both time periods indicate that postseismic deformation is consistent with deep afterslip occurring below the coseismic rupture zone. Repeated measurements of this network will be made in order to refine our velocity estimate and to continue to monitor the temporal evolution of the postseismic transient.

Acknowledgments

Many people assisted in collecting the survey-mode GPS data. We thank Ken Austin, David Bowman, Stan Cindrity, Andrea Donnellan, Don Elliott, Greg Lyzenga, David Mencin, Ben Pauk, Yufang Rong, Paul Schultz, Michelle Smith, Allan Tucker, the USGS field crew, Matt VanDomselaar, Hanbiao Wang, Min Wang, Kris Weaver, and Lupei Zhu for their time and effort. We thank Karl Gross of the USGS and the Marines at MCAGCC for coordinating work on the Marine base. We also thank people associated with SCIGN for the continuous GPS data shown here. Field work was supported by the National Science Foundation and the Southern California Earthquake Center.

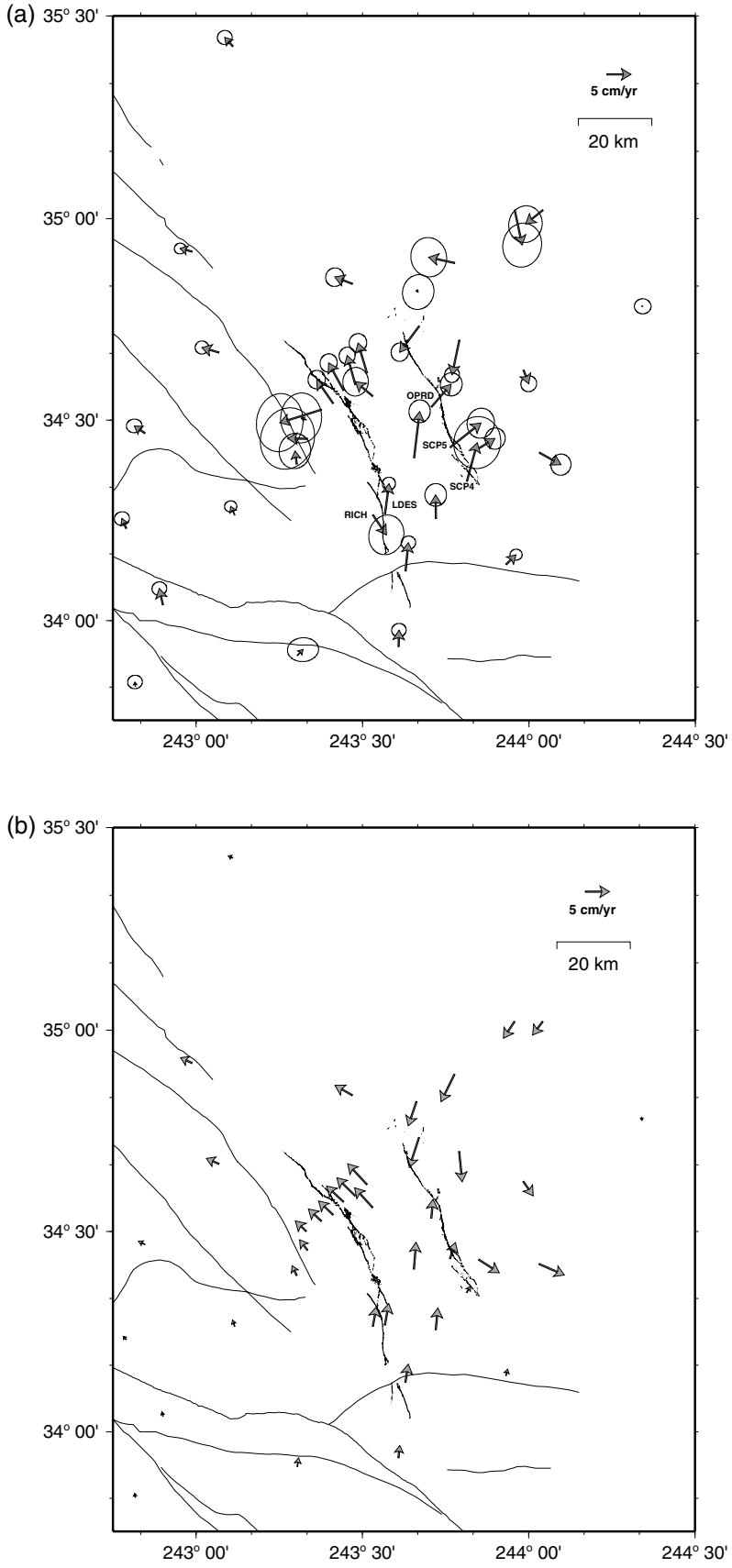

Figure 6. (*Caption on next page.*)

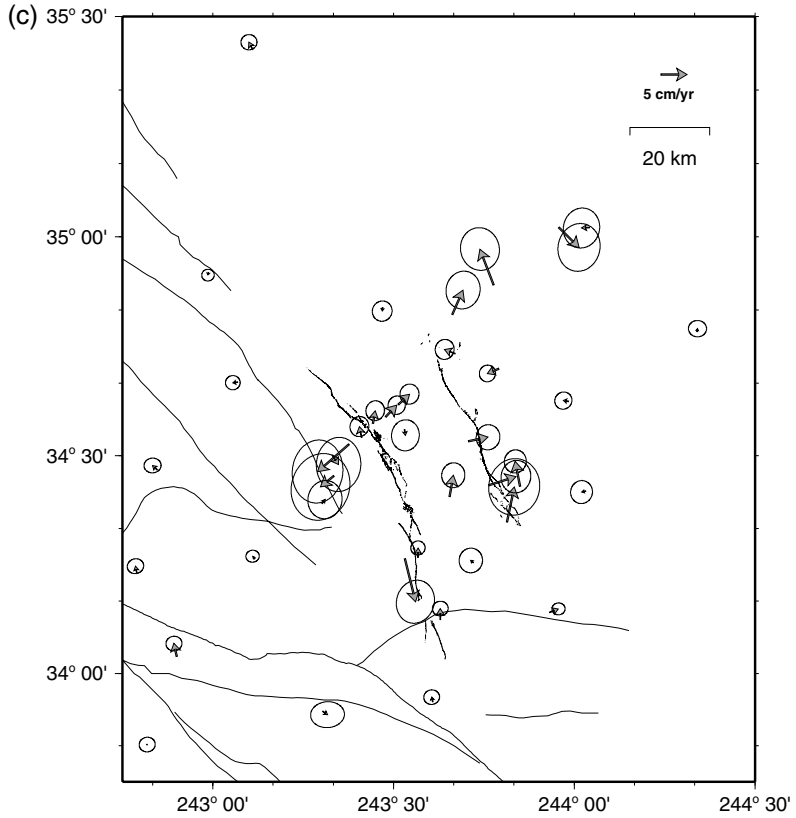

Figure 6. (a) Observed velocities from October to November 1999, minus elastic-strain accumulation along the San Andreas fault; (b) model-predicted velocities from the deep-afterslip model shown in Figure 5a; and (c) residual velocities (observed minus model predicted) from the deep-afterslip model shown in Figure 5a.

References

Agnew, D., S. Owen, Z-K. Shen, G. Anderson, J. Svarc, H. Johnson, K. Austin, and R. Reilinger (2002). Coseismic displacements from the Hector Mine earthquake: results from survey-mode GPS measurements, *Bull. Seism. Soc. Am.* **92,** 1355–1364 (this issue).

Boucher, C., Z. Altamimi, and P. Sillard (1999). The 1997 international terrestrial reference frame, in *IERS Technical Note 27*, Obs. de Paris, Paris.

Deng, J., M. Gurnis, H. Kanamori, and E. Hauksson (1998). Viscoelastic flow in the lower crust after the 1992 Landers, California, earthquake, Science **282,** 1689–1692.

Harris, R., and P. Segall (1987). Detection of a locked zone at depth on the Parkfield, California, segment of the San Andreas fault, *J. Geophys. Res.* **92,** 7945–7962.

Hauksson, E., L. M. Jones, and K. Hutton (2002). The 1999 M_w 7.1 Hector Mine, California, earthquake sequence: complex conjugate strike-slip faulting, *Bull. Seism. Soc. Am.* **92,** 1154–1170 (this issue).

Hudnut, K. W., N. E. King, J. E. Galetzka, K. F. Stark, J. A. Behr, A. Aspiotes, S. van Wyk, S. Dockter, and F. Wyatt (2002). Continuous GPS observations of postseismic deformation following the 16 October 1999 Hector Mine earthquake (M_w 7.1), *Bull. Seism. Soc. Am.* **92,** 1403–1422 (this issue).

Hurst, K., D. Argus, A. Donnellan, M. Heflin, D. Jefferson, and G. Lyzenga (2000). The coseismic geodetic signature of the 1999 Hector Mine earthquake, *Geophys. Res. Lett.* **27,** 2733–2736.

Lindvall, S., R. Rockwell, D. Schwartz, T. Dawson, J. Helms, C. Madden, D. Yule, H. Stenner, D. Raona, G. Kasman, M. Seim, A. Meltzner, and M. Caffee (2001). Paleoseismic investigations of the 1999 M 7.1 Hector Mine earthquake surface rupture and adjacent Bullion fault, Twentynine Palms Marine Corps Base, California (abstracts with programs), *Geol. Soc. Am.* **33,** 79.

Okada, Y. (1985). Surface deformation due to shear and tensile faults in a half-space, *Bull. Seism. Soc. Am.* **75,** 1135–1154.

Peltzer, G., P. Rosen, F. Rogez, and K. Hudnut (1998). Poroelastic rebound along the Landers 1992 earthquake surface rupture, *J. Geophys. Res.* **103,** no. B12, 30,131–30,145.

Pollitz, F. F., G. Peltzer, and R. Burgmann (2000). Mobility of continental mantle: evidence from postseismic geodetic observations following the 1992 Landers earthquake, *J. Geophys. Res.* **105,** 8035–8054.

Price, E. J. and D. T. Sandwell (1998). Small-scale deformations associated with the 1992 Landers, California, earthquake mapped by synthetic aperture radar interferometry phase gradients, *J. Geophys. Res.* **103,** 27,001–27,016.

Reilinger, R. E., S. Ergintav, R. Bürgmann, S. McClusky, O. Lenk, A. Barka, O. Gurkan, L. Hearn, K. L. Feigl, R. Cakmak, B. Aktug, H. Ozener, and M. N. Toksoz (2000). Coseismic and postseismic fault slip for the 17 August 1999, M = 7.5, Izmit, Turkey earthquake, *Science* **289,** 1519–1524.

Rockwell, T. K., S. Lindvall, M. Herzberg, D. Murbach, T. Dawson, and G. Berger (2000). Paleoseismology of the Johnson Valley, Kickapoo, and Homestead Valley faults: clustering of earthquakes in the eastern California shear zone, *Bull. Seism. Soc. Am.* **90,** 1200–1236.

Rymer, M. J., G. G. Seitz, K. D. Weaver, A. Orgil, G. Faneros, J. C. Hamilton, and C. Goetz (2002). Geologic and paleoseismic study of the Lavic Lake fault at Lavic Lake Playa, Mojave Desert, southern California, *Bull. Seism. Soc. Am.* **92,** 1577–1591 (this issue).

Savage, J. C. (1990). Equivalent strike-slip earthquake cycles in half-space

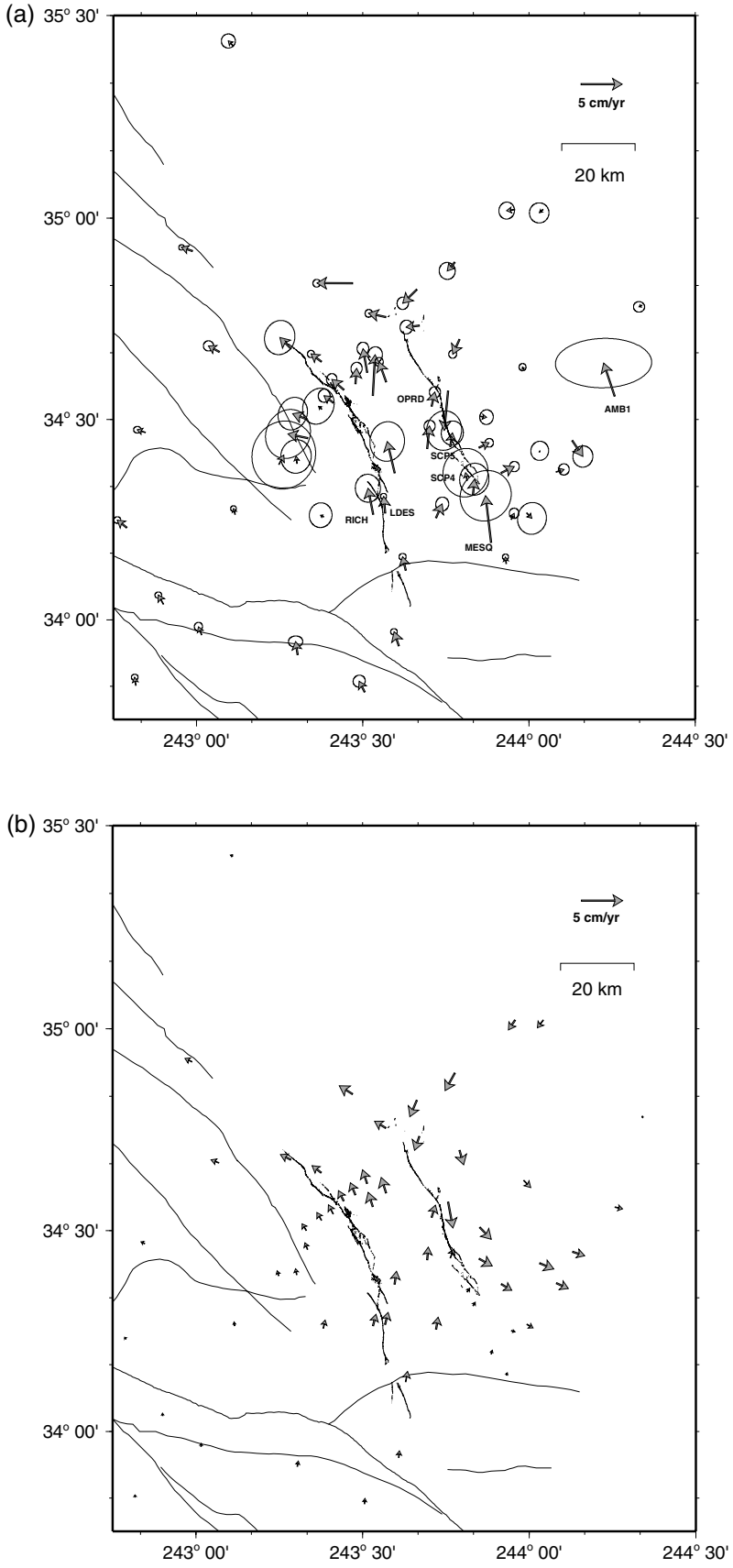

Figure 7. (*Caption on next page.*)

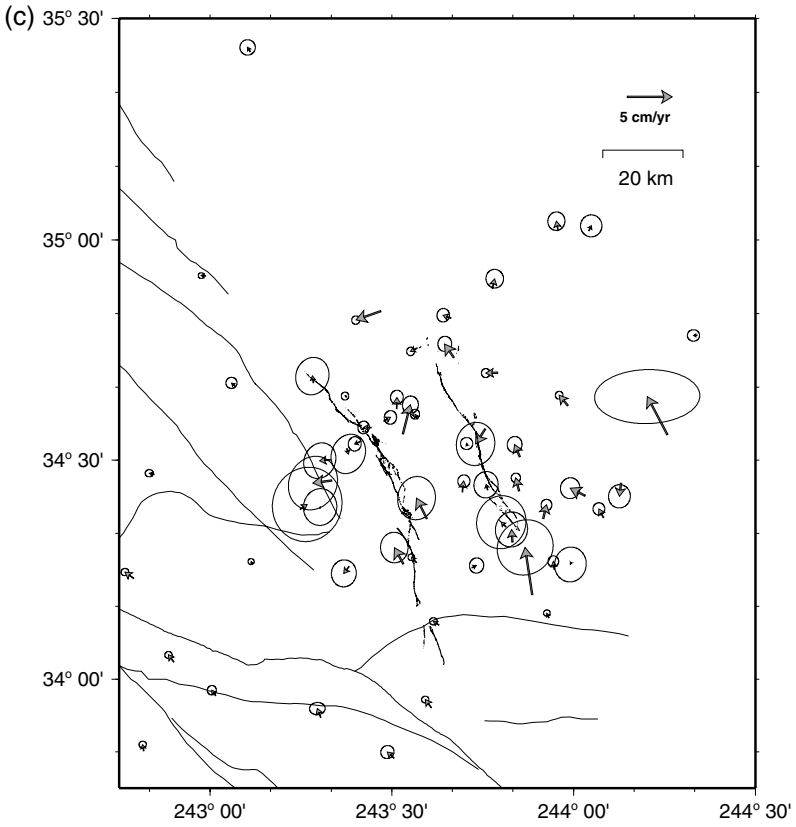

Figure 7. (a) Observed velocities from November 1999 to March 2000, minus elastic-strain accumulation along the San Andreas fault; (b) model-predicted velocities from the deep-afterslip model shown in Figure 5b; and (c) residual velocities (observed minus model predicted) from the deep-afterslip model shown in Figure 5b.

and lithosphere-asthenosphere earth models, *J. Geophys. Res.* **95,** 4873–4879.

Savage, J. C. and J. L. Svarc (1997). Postseismic deformation associated with the 1992 M_w = 7.3 Landers earthquake, southern California, *J. Geophys. Res.* **102,** 7565–7577.

Shen, Z. K., D. D. Jackson, Y. Feng, M. Cline, M. Kim, P. Feng, and Y. Bock (1994). Postseismic deformation following the Landers earthquake, California, 28 June 1992, *Bull. Seism. Soc. Am.* **84,** 780–791.

Stark, P. B. and R. L. Parker (1995). Bounded-variable least-squares: an algorithm and applications, *Comput. Statist.* **10,** no. 2.95.

Treiman, J. A., K. J. Kendrick, W. A. Bryant, T. K. Rockwell, and S. F. McGill (2002). Primary surface rupture associated with the M_w 7.1 16 October 1999 Hector Mine earthquake, San Bernardino County, California, *Bull. Seism. Soc. Am.* **92,** 1171–1191 (this issue).

Zumberge, J. M. H., D. Jefferson, M. Watkins, and F. Webb (1997). Precise point positioning for the efficient and robust analysis of GPS data from large networks, *J. Geophys. Res.* **102,** 5005–5017.

Department of Earth Sciences
University of Southern California, Los Angeles, CA
(S.O.)

Institute of Geophysics and Planetary Physics
University of California, San Diego
La Jolla, CA
(G.A., D.C.A.)

Jet Propulsion Laboratory
Pasadena, CA
(K.H.)

Earth Resources Laboratory
Massachusetts Institute of Technology
Cambridge, MA
(R. R.)

Department of Earth and Space Sciences
University of California, Los Angeles
Los Angeles, CA
(Z.-K.S.)

United States Geological Survey
Menlo Park, CA
(J.S.)

Department of Earth, Atmospheric, and Planetary Sciences
Massachusetts Institute of Technology
Cambridge, MA
(T.B.)

The Prediction Company
Sante Fe, NM
(H.J.)

Manuscript received 10 April 2001.